PAPER

Check for updates

Structure-modulated CaFe-LDHs with superior simultaneous removal of deleterious anions and corrosion protection of steel rebar†

Ji Young Park,*[a] Jimin Lee,[a] Minseob Lim,[a] Gwang-Myeong Go,[a] Hong-Baek Cho,[a] Han-Seung Lee[b] and Yong-Ho Choa [ID][a]

The three anionic species; chloride (Cl^-), sulfate (SO_4^{2-}), and carbonate (CO_3^{2-}), are typical chemical factors that environmentally accelerate failure of concrete structures with steel rebar through long-term exposure. Efficient removal of these deleterious anions at the early stage of penetration is crucial to enhance the lifespan and durability of concrete structures. Here, we synthesize CaFe-layered double hydroxide (CaFe-LDHs) by a simple one-step co-precipitation technique and structural modulation by calcination process. It is applied for the removal of Cl^-, SO_4^{2-}, and CO_3^{2-} anions as well as corrosion inhibition on steel rebar in aqueous solutions. The synthesized CaFe-LDHs with phase transfer show notable improvement of removal capacity (Q_{max}) toward Cl^- and SO_4^{2-} over 3.4 times and over 5.69 times, respectably, then those of previous literatures. Furthermore, the steel rebar exposed to an aqueous solution containing the three anionic sources shows a fast corrosion rate (1876.56×10^{-3} mm per year), which can be remarkably inhibited showing 98.83% of corrosion inhibition efficiency when it is surrounded by those CaFe-LDHs. The novel adsorption mechanisms of these CaFe-LDHs-induced crystals and corresponding corrosion protection properties are elucidated drawing on synergy of memory effects and chemical reactions.

1. Introduction

Building in concrete structures with steel rebar was a remarkable innovation in the construction industry because it adds strength to concrete, providing durability and allowing more specialized designs.[1] However, it is always exposed to corrosion, leading to deterioration in concrete structures, which determines their durability and life span, particularly in natural environments.[2,3] In general, concrete structures present good durability to corrosion because the structure of concrete presents high alkalinity in the pores of the surrounding concrete, forming a protective, passive layer on the surface of the steel rebar.[4-6] Nevertheless, corrosion of steel rebar can be readily initiated when passivity is compromised by damage[7] or when the bond between concrete and steel rebar is destroyed by anionic species. Three major anions from different sources are particularly harmful: chloride (Cl^-), sulfate (SO_4^{2-}), and carbonate (CO_3^{2-}) anions.[8] Corrosion is generally initiated by electrochemical flow of electrons and ions.[9,10]

[a]Materials Science and Chemical Engineering, Hanyang University, Ansan 15588, Republic of Korea. E-mail: Choa15@hanyang.ac.kr

[b]Department of Architectural Engineering, Hanyang University, Ansan, 15588, Republic of Korea

† Electronic supplementary information (ESI) available. See DOI: 10.1039/d1ra00300c

Penetration of Cl^- anions to reinforced concrete is significantly detrimental, especially for structures near marine environments exposed to high concentrations of salts.[11,12] In this case, the Cl^- anion can easily penetrate concrete structures through capillary adsorption, hydrostatic pressure, or diffusion, accelerating steel rebar corrosion (eqn (1)).[13,14] It can penetrate into concrete in diverse forms drawing on the chemical sources of SO_4^{2-} anions from the environment, which also promotes corrosion of steel rebar in concrete.[15] SO_4^{2-} anion attack occurs by diverse forms drawing on chemical sources, including seawater, acid rain, or combustion gas from industry, leading to destruction of the original properties of concreate (eqn (2)).[16-18] Carbonation occurs by CO_3^{2-} anions, which originate from carbon dioxide, diffusing into the concrete matrix from the air, reacting with calcium hydroxide to form calcium carbonate. This lowers pH and causes general internal volume expansion in the concentrate. When the concrete is neutralized and water and air infiltrate, the corrosion of steel and the volume expands, causing cracks in the concrete cover, resulting in loss of the strength and durability of the structure (eqn (3)).[19] This deteriorates the life-span of the concrete structures by providing easy penetration paths for other corrosion species.

$$Fe^{2+} + 2Cl^- \rightarrow FeCl_2 + 2e^- \tag{1}$$

$$2Fe + 2H_2SO_4 + O_2 \rightarrow 2FeSO_4 + 2H_2O \tag{2}$$

$$Ca(OH)_2 + CO_2 \rightarrow CaCO_3 + H_2O \qquad (3)$$

Deterioration in performance or structural damage of reinforced concrete structures not only adversely affects safety, but also causes enormous losses to society and the national economy over a long period of time.[20,21] Therefore, it is necessary to selectively and promptly remove deleterious anions as soon as they penetrate the concrete structure to maintain durability and life span.

Layered double hydroxides (LDHs) are hydrotalcite-like compounds with high specific surface area, memory effects, eco-friendly features, and low-cost, widening utilization in the fields of hazardous materials adsorption, catalysts, biomedicine, agriculture, and wastewater treatment.[22–25] The general formula of LDHs is $[M_{1-x}^{2+}M_x^{3+}(OH)_2]_x^+[A^{n-}]_{x/n} \cdot yH_2O$, where M^{2+} includes Ca, Mg, Zn, Co, Ni, and Cu, and M^{3+} includes Fe, Al, and Cr. LDHs are composed of positively charged layers with divalent and trivalent metal cations, and interlayer anions (A^{n-}) is a negatively charged anion layer. The layer structures of positive charges are balanced by the A^{n-}, which are exchangeable with other anionic species in aqueous solutions.[26] In addition, the crystallinity of LDHs can typically be transformed into their respective metal oxides by calcining at temperatures in the range of 400 to 700 °C. As a consequence, water in the crystals, hydroxyl groups of LDHs, and intercalated anions are completely removed, leaving behind mixed metal oxides. It is a unique property of LDH that it recovers its original structure after calcination followed by reconstruction *via* the memory effect.[27,28] Compared to most frequently used MgAl-based LDHs (MgAl-LDHs), CaFe-based LDHs (CaFe-LDHs) are synthesized in a cost-effective way by co-precipitation at room temperature without increasing the reaction temperature.[29,30] Although much work has been reported on the corrosion inhibitive effects of LDHs,[31–34] the influence of co-existing Cl^-, SO_4^{2-}, and CO_3^{2-} anions on the corrosion protection ability of LDHs has not been considered. Moreover, few studies have investigated the anion adsorption mechanisms of CaFe-based LDHs and their potential for corrosion resistant property.

In this study, we report a synthesis of CaFe-LDHs and CaFe-based metal oxides by a modified one-step co-precipitation method follow by structural modulation. The removal performance of harmful anionic species including Cl^-, SO_4^{2-}, and CO_3^{2-} are studied in an aqueous solution containing the nanopowders, initiated by the CaFe-LDHs. The corrosion protection efficiency of steel rebar for the potential improvement of the durability of concrete structures is envisaged relying on structural variation of the CaFe-LDHs. The mechanisms for simultaneous capturing of anion species and anti-corrosion are investigated with respect to phase transfer of CaFe-LDHs drawing on the variation of crystallinity coupled with stoichiometry.

2. Experimental

2.1. Materials and reagents

Reagents were prepared using calcium nitrate tetrahydrate ($Ca(NO_3)_2 \cdot 4H_2O$, 99%), iron nitrate nonahydrate ($Fe(NO_3)_3 \cdot 9H_2O$, 98%), sodium hydroxide (NaOH, 99%), sodium chloride (NaCl, 99.5%), sodium sulphate (Na_2SO_4, 99%), and sodium carbonate (Na_2CO_3, 99.5%). All were as-purchased from Sigma-Aldrich, Inc. Daejung, Inc. without further purification. Distilled deionized water was used for preparation of aqueous standard ionic solutions.

2.2. Synthesis of CaFe-LDHs

CaFe-LDHs, which were previously prepared by a typical co-precipitation method,[30,35,36] were prepared *via* a modified method here. Specifically, CaFe-LDH was prepared by one-step synthesis of co-precipitation of two precursor materials, an aqueous solution containing 3 M NaOH (900 mL) was rapidly injected into the second solution (900 mL) containing a mixture of 66.7 mmol of $Ca(NO_3)_2 \cdot 4H_2O$ and 33.3 mmol of $Fe(NO_3)_3 \cdot 9H_2O$ at room temperature for 1 min (900 mL min^{-1}) and the solution was then aged for 18 h. The concentration was balanced corresponding to fixed molar ratios of $Ca^{2+} : Fe^{3+}$ (2 : 1). During this process, the pH was maintained at 13, and the reaction was always performed at room temperature (25 °C). Then, the synthesized CaFe-LDHs were washed with excess quantities of ethanol to remove unwanted nitrate salt.

2.3. Structural transformation of CaFe-LDHs

Structural transformation of CaFe-LDHs was carried out by a calcination process. The calcined CaFe-LDHs were prepared under two heat treatment conditions of the original LDHs in a furnace at 400 °C (C-400 LDHs) and 700 °C (C-700 LDHs) for 3 h in an air atmosphere. Both the un-calcined (pristine LDHs) and calcined LDHs were ground prior to analysis or use in adsorption experiments.

2.4. Adsorption test of ionic species in aqueous phase by CaFe-LDHs

(1) Removal of Cl^- by CaFe-LDHs. The Cl^- solution was prepared by dissolving NaCl in deionized water. The initial concentration of Cl^- was 200 ppm. The Cl^- removal was then carried out by adding 1.89 g of pristine, C-400 and C-700 LDHs in 200 mL of the aqueous ionic solution at pH 7.

(2) Removal of SO_4^{2-} by CaFe-LDHs. The SO_4^{2-} solution was prepared by dissolving Na_2SO_4 in deionized water. The initial concentration of SO_4^{2-} was 100 ppm. The SO_4^{2-} removal was then carried out by adding 0.472 g of pristine, C-400 and C-700 LDHs in 200 mL of the aqueous ionic solution at pH 7.

(3) Removal of CO_3^{2-} by CaFe-LDHs. The CO_3^{2-} solution was prepared by dissolving Na_2CO_3 in deionized water. The initial concentration of CO_3^{2-} was 100 ppm. The CO_3^{2-} removal was then carried out by adding 0.505 g of pristine, C-400 and C-700 LDHs in 200 mL of the aqueous ionic solution at pH 7.

Removal of anions in the aqueous solution was conducted by anion exchange reactions during solution mixing assisted by magnetic stirring at 250 rpm, and propagation of the reaction was monitored by analyzing the LDH solution after sampling at adsorption times of 5, 10, 20, 30, and 60 min. The collected solutions were filtered with a 0.20 micro filtration membrane to

separate the LDHs from solution. The solid powder was then dried at 100 °C for 3 h in a vacuum oven for further analysis.

2.5. Competitive adsorption test of ionic species in aqueous phase by CaFe-LDHs

The anionic solution with Cl^-, SO_4^{2-}, and CO_3^{2-} was prepared by dissolving NaCl, Na_2SO_4, and Na_2CO_3 in deionized water. The initial concentrations of Cl^-, SO_4^{2-}, and CO_3^{2-} anions were all 250 ppm. Adsorption was carried out by adding 1 g of pristine, C-400 LDHs, or C-700 LDHs in 200 mL of the aqueous ionic solution at pH 7. Removal of anions in the aqueous solution was monitored as described in Section 2.4.

2.6. Corrosion protection test of steel rebar by direct contact with Cl^-, SO_4^{2-}, and CO_3^{2-} anions in an aqueous solution with/without CaFe-LDHs

A steel rebar, which had a chemical composition (in wt%) of 0.27 C, 0.90 Mn, 0.20 Cu, 0.05 S, 0.04 Si, and 0.04 P (Fe balance),[37] was used in the corrosion experiments. The steel rebar (1.5 mm diameter) was cleaned with ethanol. The test specimen was further coated with a micro-stop coating with a 1 × 1 cm^2 exposed area to carry out corrosion measurements. Electrolyte solutions were prepared with 250 ppm of NaCl, Na_2SO_4, and Na_2CO_3 solutions, respectively. Corrosion effects were analyzed with/without LDHs (1 g) of various structural transformations. Corrosion was monitored as a function of time by adding 1 g of the structure modulated CaFe-LDHs powders into 200 mL corrosion solutions. The saturated calomel electrode (SCE), platinum electrode (PE) and CaFe-LDHs were connected to reference, counter electrode and working electrodes, respectively. For corrosion testing, the anti-corrosive properties and electrical conductivity of the rebar were determined by electrochemical measurements, including potentiodynamic polarization (PDP) and electrochemical impedance spectroscopy (EIS). The EIS measurements were carried out by applying a sinusoidal potential perturbation of 10 mV over a frequency range of 100 kHz to 10 mHz. The obtained EIS spectra were analyzed with an equivalent circuit using Zman software (WonATech Co. Ltd., Republic of Korea). All electrochemical measurements were performed under quiescent conditions. No attempt was made to aerate or deaerated the test solutions.

2.7. Characterization

The pH was measured using an FE20 pH meter (Mettler Toledo, USA) equipped with a glass electrode (LE438, Mettler Toledo, USA). Concentrations of exchanged liquid were determined by ion chromatography (METROSEP A SUPP 5-250) at a flow rate of 0.7 mL min^{-1} with an eluent mixture of 3.2 mM Na_2CO_3/1.0 mM $NaHCO_3$. The solid sample was characterized by Fourier transform infrared spectroscopy (FT-IR) (Thermo, Scientific 380 FT-IR) in the range of 4000 to 500 cm^{-1} with resolution of 4 cm^{-1}. X-ray diffraction (XRD) patterns of solid were obtained on a D/max2200 diffractometer (Rigaku Co., Japan) with Cu Kα radiation ($\lambda = 0.15406$ nm) operating at 40 kV and 100 mA in the range of $2\theta = 10$–80° at a scan speed of 4° min^{-1}. The

morphology of the solid was characterized by scanning electron microscopy (SEM, S-4800, Hitachi Ltd., Japan). The morphologies and sizes of the as-obtained samples were observed by transmission electron microscopy (TEM, JEM-2100F, JEOL, Japan) at 200 kV to obtain high-resolution images.

3. Results and discussion

3.1. Characterization of CaFe-LDHs by structural transformation

XRD patterns of the as-synthesized Pristine LDHs and their modulated structures are displayed in Fig. 1. The pristine LDHs were confirmed as CaFe-LDHs with crystallinity associated with $Ca_2Fe(OH)_6(NO_3)\cdot2H_2O$, which is intercalated with NO_3^- anions and crystalline water exhibiting a hexagonal structure (JCPDS no. 48-65). The diffraction peaks are located at 10.12°, 20.40°, and 30.28°, corresponding to the (001), (002), and (110) planes, respectively.[38,39] Obvious phase changes were observed for CaFe-LDHs calcined at different temperatures. The original structure of pristine LDH was destroyed and transformed into $Ca_2Fe_2O_5$ (JCPDS no. 47-1744) with an orthorhombic structure. Subsequently, $CaCO_3$ (JCPDS no. 86-2339), indexed to a rhombohedral structure with a main diffraction peak at $2\theta = 29.36°$, was newly generated. This can be caused by a small amount of CO_2 dissolution from air during the calcination process.[40–42] As the calcination temperature increased, the $CaCO_3$ phase disappeared, and crystallization of the CaO phase increased. When the temperature exceeded 550 °C, decomposition ensued. The disappearance of $CaCO_3$ was explained by the following reaction [eqn (4)]:

$$CaCO_{3(s)} \rightarrow CaO_{(s)} + CO_{2(g)} \qquad (4)$$

The FT-IR spectra of CaFe-LDHs were analyzed to identify the structural transformation by comparing chemical bonding of functional groups (ESI 1†). The characteristic peak at 1640 cm^{-1} corresponds to the H–O–H bending vibration of the interlayer water in the crystalline structure, and the characteristic sharp absorption band at around 1350 cm^{-1} is the asymmetric stretching mode of NO_3^- in the interlayer (ESI 1(b)†). The intense broad bands observed at 3585 cm^{-1} are associated with stretching vibrations of structural OH^- groups in $Ca(OH)_2$ and $Fe(OH)_2$ (ESI 1(c)†). The peaks at 749 and 580 cm^{-1} are
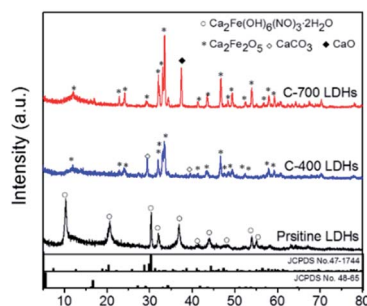

Fig. 1 XRD patterns of CaFe-LDHs with different structural transformations for pristine LDHs, C-400 LDHs, and C-700 LDHs.
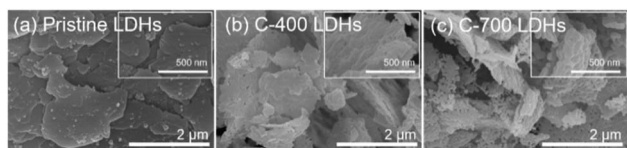
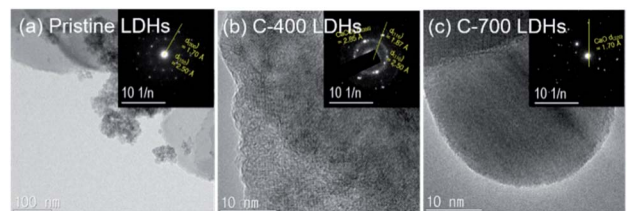Fig. 2 SEM images of (a) pristine LDHs, (b) C-400 LDHs, and (c) C-700 LDHs.

Fig. 3 TEM images and SAED patterns of (a) pristine LDHs, (b) C-400 LDHs, and (c) C-700 LDHs.
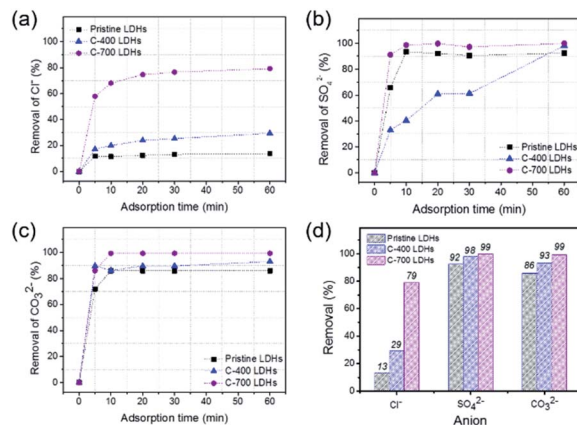

Fig. 4 Ion chromatograph of removal performance of CaFe-LDHs: pristine LDHs, C-400 LDHs, and C-700 LDHs, toward different adsorption anions: (a) Cl^-, (b) SO_4^{2-}, and (c) CO_3^{2-} as a function of reaction interaction time toward anions, and (d) anion removal percentage toward anionic species at a fixed adsorption time (at 60 min).

attributed to stretching vibrations of Ca–O or Fe–O (metal–O) in lattices as shown in ESI 1(d).†[43,44] Because the crystallized water molecules were removed, the band at 1640 cm^{-1} became weaker after calcination and completely decomposed in the case of C-400 LDHs. The gradual decrease of NO_3^- stretching vibration intensity at 1350 cm^{-1} also implies decomposition of the NO_3^- anion, which was completely decomposed in C-700 LDHs. The noticeable decrease in OH^- groups in C-400 LDHs implies that the OH^- groups of cationic layers, such as $Ca(OH)_2$ and $Fe(OH)_2$, decomposed during thermal treatment at 400 °C. Subsequently, the peak intensity increase of Ca–Fe–O at 749 and 580 cm^{-1} indicates that the pristine LDHs transformed into oxidized metal oxide structures. The commercial $CaCO_3$ peaks were observed at 1394 cm^{-1} (v_3 asymmetric CO_3^{2-}) along with a sharp band at 871 cm^{-1} (v_2 asymmetric CO_3^{2-}).[45] Those bands decreased in peak intensity with increasing calcination temperature from 400 °C to 700 °C, and a structural transformation occurred at the C-400 LDHs based on XRD data.

Fig. 2 shows the Scanning electron microscopy (SEM) images of Pristine LDHs, C-400 LDHs and C-700 LDHs. As shown, the morphology of C-400 LDHs changed from a smooth surface into one with more roughness and pores because the water of crystallization and the interlayer anions were removed by transformation from pristine LDHs to a metal oxide phase. This morphology change distinctly appears and consists primarily of individual spherical particles in C-700 LDHs, which is related to transformation of $CaCO_3$ to CaO. In addition, the lateral particle size of CaFe-LDHs confirmed about 1 μm of pristine LDHs, about 500 nm of C-400 LDHs and about 300 nm of C-700 LDHs. The particle size is an important factor regarding anion exchange.[46]

Fig. 3 displays the transmission electron microscopy (TEM) images and associated Selected area diffraction (SAED) patterns of CaFe-LDHs. Pristine LDHs revealed the typical crystallographic layered structure of CaFe-LDHs, which had SAED patterns revealing the (300) and (103) planes with lattice constants of 1.70 Å and 2.50 Å. However, C-400 LDHs indicated the existence of the (006), (110), and (116) planes corresponding

to a $CaCO_3$ rhombohedral structure after thermal treatment at 400 °C. The unique thermal treatment-induced by-product, CaO, was confirmed in C-700 LDHs, and it was identified in XRD as shown in Fig. 1. Thus, the SEAD patterns validate the gradual structural and crystallographic transitions as a function of temperature from 400 to 700 °C.

3.2. Performance and mechanism of Cl^-, SO_4^{2-}, and CO_3^{2-} anion adsorption by CaFe-LDHs

An experiment was conducted to test the simultaneous removal of deleterious anions found in aggressive natural environments. Fig. 4 shows the removal of Cl^-, SO_4^{2-}, and CO_3^{2-} anions by applying different types of CaFe-LDHs (pristine LDHs, C-400 LDHs and C-700 LDHs) for 60 min. The percentage removal efficiency was estimated according to eqn (5).

$$Removal\ (\%) = \frac{C_0 - C_e}{C_0} \times 100 \quad (5)$$

where C_0 and C_e are the initial and equilibrium anion concentration (mg L^{-1}), respectively.
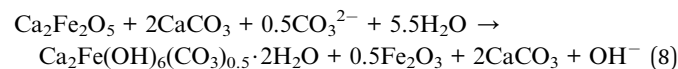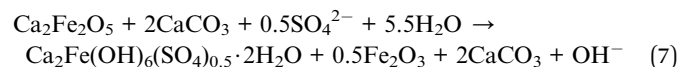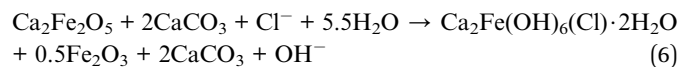
As shown in Fig. 4(a), the removal (%) of Cl^- anions by pristine LDHs, C-400 LDHs, and C-700 LDHs was 13%, 16.98%, and 57.90%, respectively, for 5 min-adsorption time at the initial stage of reaction. The removal of Cl^- anions gradually increased at 60 min and reached 13.41% for pristine LDHs, 29.25% for C-400 LDHs, and 79.62% for C-700 LDHs. The removal efficiency by C-700 LDHs was 5.94 times the corresponding value of pristine LDHs, indicating outstanding removal ability of Cl^- anions. The effect of SO_4^{2-} anion removal by employing the CaFe-LDHs is shown in Fig. 4(b). The results show that removal of SO_4^{2-} anions rapidly increased from 0% to 65.80% for pristine LDHs, 32.96% for C-400 LDHs, and 91% for C-700 LDHs for just 5 min of initial adsorption. The values then reached 92.25% (pristine LDHs), 98.07% (C-400 LDHs), and 99.86% (C-700 LDHs) when adsorption was complete after 60 min. As shown in Fig. 4(c), the removal of CO_3^{2-} anions was faster than other anion species for all the
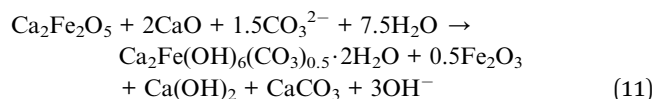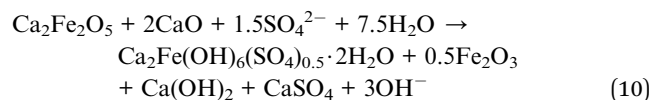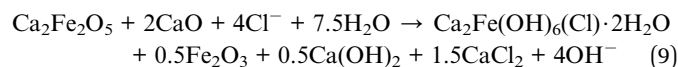
tested LDHs. C-700 LDH exhibited almost 100% of carbonate removal after 10 minutes of anion adsorption. Consequently, C-700 LDHs showed the highest removal efficiency toward Cl^-, SO_4^{2-}, and CO_3^{2-} anions, with values of 79.62%, 99.86%, and 99.30%, respectively (Fig. 4(d)).

The FT-IR spectra of CaFe-LDHs including (a) pristine LDHs, (b) C-400 LDHs, (c) C-700 LDHs and their post-adsorption samples after uptake-tests of Cl^-, SO_4^{2-}, and CO_3^{2-} anions are shown in ESI 2.† In the spectrum of the pristine LDHs (ESI. 2(a)†), adsorption peaks at 1360, 1116, and 1480 cm^{-1} can be attributed to Cl^-, SO_4^{2-}, and CO_3^{2-} interlayer anion stretching, respectively.[43,47,48] Typical CaFe-LDHs peaks were observed at 580 and 749 cm^{-1} in the spectrum of all samples as well as metal–O at 1640 cm^{-1} for H–O–H and 3585 cm^{-1} for hydroxyl groups in $Ca(OH)_2$ and $Fe(OH)_2$ after anion adsorption. C-400 LDHs and C-700 LDHs (ESI. 2(b) and (c)†) not subjected to the anion adsorption test showed typical H–O–H peaks of bending vibration (1360 cm^{-1}) and stretching vibration (3585 cm^{-1}) induced by hydroxyl groups, which were removed during heating. However, the adsorption peaks returned after adsorption of Cl^-, SO_4^{2-}, and CO_3^{2-} anions because the hydroxyl groups and water from crystallization were recovered by a refolding process that occurs in an aqueous atmosphere. Thus, there is good evidence of successful adsorption of the three anions (Cl^-, SO_4^{2-}, and CO_3^{2-}) and reconstruction processes of CaFe-LDHs.

Reconstructed CaFe-LDHs were characterized by XRD after 60 min-adsorption tests with anions Cl^-, SO_4^{2-}, and CO_3^{2-} anions as shown in ESI 3.† The characteristic diffractions of typical CaFe-LDHs were recognized as rhombohedral structures in all LDHs samples, including plane (006) and (0012) after adsorption of Cl^-, SO_4^{2-}, and CO_3^{2-} anions. The crystalline LDHs structures corresponded to $Ca_2Fe(OH)_6(Cl)\cdot 2H_2O$ (JCPDS no. 44-445) after Cl^- adsorption, $Ca_2Fe(OH_6)(SO_4)_{0.5}\cdot 3H_2O$ (JCPDS no. 44-448) after SO_4^{2-} adsorption, and $Ca_2Fe(OH_6)(CO_3)_{0.5}\cdot 3H_2O$ (JCPDS no. 43-480) after CO_3^{2-} adsorption. Simultaneously, the crystallinity of the CaFe-LDHs decreased with anion adsorption due to the reconstruction phenomenon, which is the so called memory effect.[49,50] As shown in ESI 3(a),† the basal spacing decreased, and the 2θ on the (006) plane increased from 10.36° (NO_3^-) to 11.32° (Cl^-) because the anion ionic radius of Cl^- (1.75 Å) was smaller than that of the NO_3^- (1.79 Å). The Cl^- anion was partially substituted with NO_3^- present in the interlayer, which led to two types of interstratified pristine LDHs. Also, the 2θ on the (006) plane of CO_3^{2-} interlayered LDH (11.64°) was higher than that of pristine LDHs.[51] In a continuation of the pre-adsorption measurements shown in Fig. 1, post-adsorption C-400 LDHs also included secondary crystalline phases of $CaCO_3$ ($2\theta = 29.36°$) in all CaFe-LDHs samples even after particle reconstruction (ESI 3(b)†). This is because $CaCO_3$ is a basic salt with very low solubility in water. Interestingly, a characteristic peak of Fe_2O_3 was observed after anion adsorption with C-400 LDHs and C-700 LDHs. Moreover, the CaFe-based metal oxide, $Ca_2Fe_2O_5$, converted into CaFe-LDHs during the refolding process in an aqueous solution by intercalating anion species (Cl^-, SO_4^{2-}, and CO_3^{2-}). Therefore, C-400 LDHs refolded in aqueous solutions by exchanging anions *via* reconstruction of $Ca_2Fe_2O_5$ according to the following reactions [eqn (6)–(8)]:

$$Ca_2Fe_2O_5 + 2CaCO_3 + Cl^- + 5.5H_2O \rightarrow Ca_2Fe(OH)_6(Cl)\cdot 2H_2O + 0.5Fe_2O_3 + 2CaCO_3 + OH^- \quad (6)$$

$$Ca_2Fe_2O_5 + 2CaCO_3 + 0.5SO_4^{2-} + 5.5H_2O \rightarrow \\ Ca_2Fe(OH)_6(SO_4)_{0.5}\cdot 2H_2O + 0.5Fe_2O_3 + 2CaCO_3 + OH^- \quad (7)$$

$$Ca_2Fe_2O_5 + 2CaCO_3 + 0.5CO_3^{2-} + 5.5H_2O \rightarrow \\ Ca_2Fe(OH)_6(CO_3)_{0.5}\cdot 2H_2O + 0.5Fe_2O_3 + 2CaCO_3 + OH^- \quad (8)$$

In particular, the CaFe-LDHs prepared after thermal treatment at C-700 LDHs showed a pure crystalline structure of CaFe-LDHs with phase transformation of CaO into both a $Ca(OH)_2$ phase and $CaCl_2$, $CaSO_4$, and $CaCO_3$ phases depending on the anion species. Thus, the C-700 LDHs may undergo reconstruction *via* the following chemical reaction in water with specific anions [eqn (9)–(11)]:

$$Ca_2Fe_2O_5 + 2CaO + 4Cl^- + 7.5H_2O \rightarrow Ca_2Fe(OH)_6(Cl)\cdot 2H_2O \\ + 0.5Fe_2O_3 + 0.5Ca(OH)_2 + 1.5CaCl_2 + 4OH^- \quad (9)$$

$$Ca_2Fe_2O_5 + 2CaO + 1.5SO_4^{2-} + 7.5H_2O \rightarrow \\ Ca_2Fe(OH)_6(SO_4)_{0.5}\cdot 2H_2O + 0.5Fe_2O_3 \\ + Ca(OH)_2 + CaSO_4 + 3OH^- \quad (10)$$

$$Ca_2Fe_2O_5 + 2CaO + 1.5CO_3^{2-} + 7.5H_2O \rightarrow \\ Ca_2Fe(OH)_6(CO_3)_{0.5}\cdot 2H_2O + 0.5Fe_2O_3 \\ + Ca(OH)_2 + CaCO_3 + 3OH^- \quad (11)$$

C-400 and C-700 LDHs showed low crystallinity with individual interlayer anions of Cl^-, SO_4^{2-}, and CO_3^{2-} compared to pristine LDH. This may be related to the phase transfer of $Ca_2Fe_2O_5$ to a layer-by layer structure of CaFe-LDHs by reconstruction.

3.3. Competitive adsorption performance of CaFe-LDHs by structural transformation caused by Cl^-, SO_4^{2-}, and CO_3^{2-} anions

To evaluate the removal performance of CaFe-LDHs in a mixture of three anions (Cl^-, SO_4^{2-}, and CO_3^{2-}), competitive adsorption was studied by adding the pristine, C-400, and C-700 LDHs to an aqueous anionic solution. As shown in Fig. 5, 100% removal of
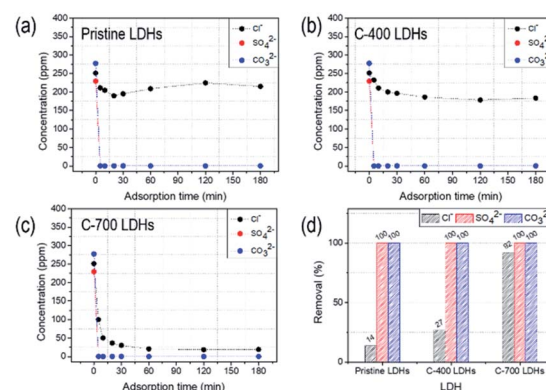

Fig. 5 Competitive adsorption toward the mixture of ionic species: Cl^-, SO_4^{2-} and CO_3^{2-} anions (a) pristine LDHs, (b) C-400 LDHs, and (c) C-700 LDHs and (d) removal percentage toward anionic species fixed adsorption 180 min.
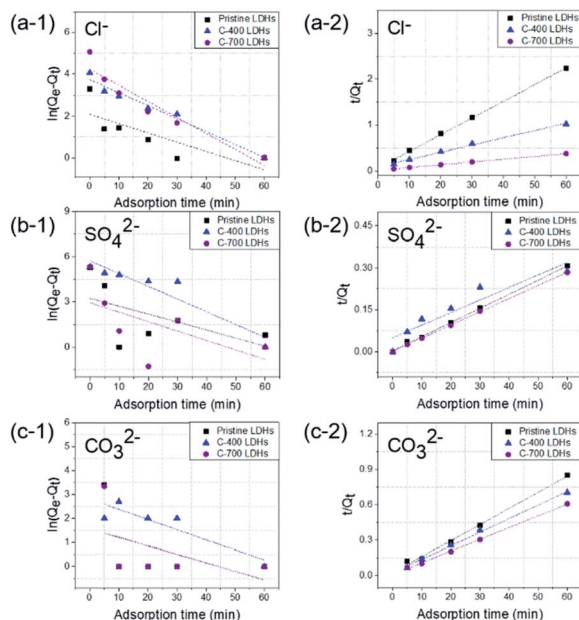
Fig. 6 (a–c) Pseudo-first-order and (a-2, b-2 and c-2) pseudo-second-order kinetic plots for sorption of CaFe-LDHs with different adsorption anions: (a-1 and a-2) Cl⁻, (b-1 and b-2) SO₄²⁻ and (c-1 and c-2) CO₃²⁻.
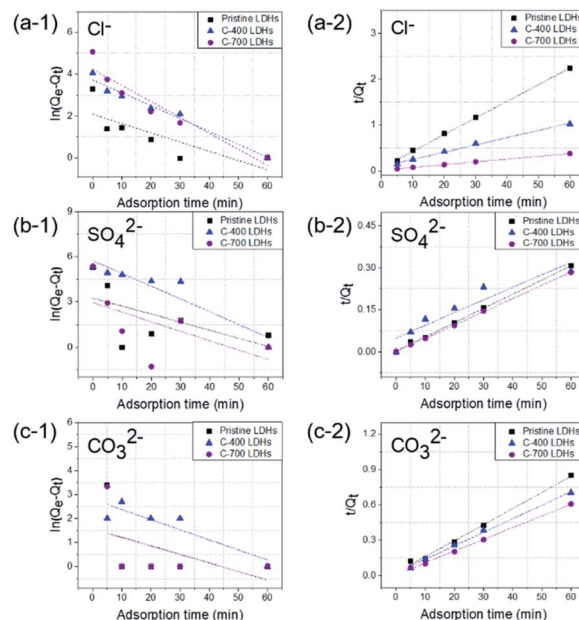

Fig. 7 (a–c) Langmuir and (a-2, b-2 and c-2) Freundlich plots for sorption of CaFe-LDHs with different adsorption anions: (a-1 and a-2) Cl⁻, (b-1 and b-2) SO₄²⁻, and (c-1 and c-2) CO₃²⁻.

SO_4^{2-} and CO_3^{2-} anions in all CaFe-LDHs was observed after 5 minutes of adsorption time. The removal performance toward Cl^- anions, however, was low after 5 min of adsorption and only reached 14.34% for pristine LDHs, 27.09% for C-400 LDHs, and 92.43% for C-700 LDHs at 180 min of adsorption time. This implies that the removal capacity of the prepared CaFe-LDHs is fastest toward SO_4^{2-} and CO_3^{2-} anions under fixed anion concentrations. The required adsorption time until adsorption saturation decreased in the order of CO_3^{2-} and SO_4^{2-} > Cl^- over 180 min of adsorption.

3.4. Adsorption kinetics of Cl^-, SO_4^{2-}, and CO_3^{2}

To investigate the differences in anion absorption performance for CaFe-LDHs, the adsorption kinetics of Cl^-, SO_4^{2-}, and CO_3^{2-} anions on CaFe-LDHs were determined by fitting the

experimental data to the linearized form of pseudo-first-order (eqn (12)) and pseudo-second-order (eqn (13)) models:

$$\ln(Q_e - Q_t) = \ln Q_e - k_1 t \tag{12}$$

$$\frac{t}{Q_t} = \frac{1}{k_2 Q_e^2} + \frac{t}{Q_e} \tag{13}$$

Here, Q_e and Q_t are the amounts of anions adsorbed (mg g⁻¹) per unit of LDHs at equilibrium and at specified time t (min), respectively. k_1 and k_2 are the pseudo-first-order and pseudo second-order rate constants, respectively. Correlation coefficients (R^2) were compared in determining the kinetic model for quantitative evaluation. The pseudo-first- and pseudo-second-order plots for sorption of anions by CaFe-LDHs as a function of adsorption time are fitted in Fig. 6, and the specific model parameters obtained toward Cl^-, SO_4^{2-}, and CO_3^{2-} anion concentrations are arranged in Table 1.
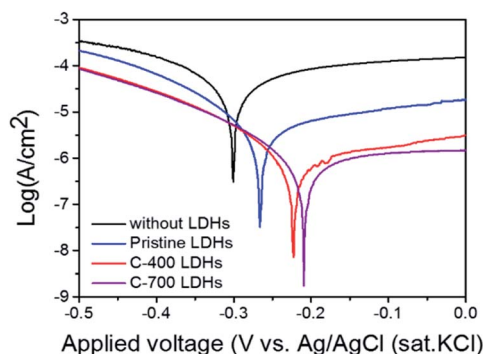
Table 1 Coefficients of pseudo-first-order and pseudo-second-order parameters for Cl^-, SO_4^{2-}, and CO_3^{2-} adsorption by CaFe-LDHs, pristine, C-400, and C-700 LDHs

Anion	LDHs	Pseudo first order kinetic parameters			Pseudo second order kinetic parameters		
		K_1 (min⁻¹)	Q_e (mg)	R^2	K_2 (mg⁻¹ min⁻¹)	Q_e (mg)	R^2
Cl^-	Pristine LDHs	0.091	3.805	0.913	0.038	14.343	0.954
	C-400 LDHs	0.060	19.950	0.892	0.001	31.849	0.974
	C-700 LDHs	0.106	32.621	0.810	0.001	85.294	0.957
SO_4^{2-}	Pristine LDHs	0.053	25.460	0.140	0.008	197.516	0.998
	C-400 LDHs	0.085	307.570	0.860	0.001	222.150	0.941
	C-700 LDHs	0.063	19.017	0.192	0.018	211.691	0.999
CO_3^{2-}	Pristine LDHs	0.036	2.789	0.017	0.012	73.243	0.994
	C-400 LDHs	0.042	16.367	0.762	0.006	86.885	0.996
	C-700 LDHs	0.035	4.687	0.017	0.010	100.640	0.998

Table 2 Langmuir and Freundlich isotherm parameters for Cl^-, SO_4^{2-}, and CO_3^2 adsorption by C-700 LDHs

Anion	Langmuir isotherm parameter			Freundlich isotherm parameters		
	K_L (L mg^{-1})	Q_{max} (mg)	R^2	K_F (L mg^{-1})	n	R^2
Cl^-	0.0006	881.8342	0.9988	3.1183	1.3050	0.9881
SO_4^{2-}	0.0019	706.2140	0.6964	43.8870	3.9432	0.3627
CO_3^{2-}	0.0006	879.7300	0.9999	0.8587	0.9841	0.9998

Fig. 8 Potentiodynamic polarization (PDP) curves obtained in NaCl, Na_2SO_4, and Na_2CO_3 solutions (250 ppm solution) without CaFe-LDHs and with CaFe-LDHs.

The data were very well fitted when using a pseudo-second-order plot, as shown in Table 1. The high correlation coefficient values (R^2) obtained for all the LDHs adsorbent samples confirmed that the pseudo-second-order model describing the Cl^-, SO_4^{2-}, and CO_3^{2-} anions kinetics was very well fit compared to the pseudo-first-order. Based on the kinetic parameters, the pseudo-second order model data suggest that the rate limiting step during Cl^-, SO_4^{2-}, and CO_3^{2-} anion adsorption onto CaFe-LDHs was primarily chemisorption. Therefore, chemisorption, which typically involves electrostatic attraction and chemical bonding between adsorbate and adsorbent, was the dominant factor for adsorbate anions Cl^-, SO_4^{2-}, and CO_3^{2-} onto CaFe-LDHs.[52]

3.5. Equilibrium sorption measurements and modelling

The aim of the adsorption isotherms is to correlate the adsorbate concentration in the solution and the adsorbed extent of metal ions at the adsorbate-to-adsorbent interface. Langmuir and Freundlich isotherm models were important for design of

sorption systems (Fig. 7). The adsorption of Cl^-, SO_4^{2-}, and CO_3^{2-} anions onto CaFe-LDHs (here, C-700 LDHs) was investigated, and the applicability of the isotherms described above was examined. The Langmuir model assumes that interactions occur on a homogenous surface by monolayer adsorption between ions. The Langmuir isotherm represents the equilibrium distribution of sorbate between solid and liquid phases and is often expressed as (eqn (14)):

$$Q_e = \frac{Q_{max}K_L C_e}{1 + K_L C_e} \quad (14)$$

Here, C_e (mg L^{-1}) is the concentration of sorbate at equilibrium, Q_e (mg g^{-1}) is the amount sorbed per mass of sorbent at equilibrium, K_L (L mg^{-1}) is the equilibrium constant related to the sorption energy between sorbate and sorbent, and Q_{max} (mg) is the limiting amount of sorbate that can be taken up per mass of sorbent. The Langmuir parameters were $Q_{max} = 881.83$ mg g^{-1} for Cl^-, $Q_{max} = 706.21$ mg g^{-1} for SO_4^{2-}, and $Q_{max} = 879.73$ mg g^{-1} for CO_3^{2-}.

The Freundlich equation can be used to estimate the sorption intensity of sorbent toward sorbate as [eqn (15)]:

$$Q_e = K_F C_e^{1/n} \quad (15)$$

Here, Q_e (mg g^{-1}) is the amount of sorbed anion, C_e is the equilibrium concentration, and K_F and n are constants incorporating all parameters affecting the sorption process, such as sorption capacity and intensity. The isotherm constants in eqn (14) and (15), as well as the correlation coefficients (R^2) are given in Table 2. Based on the R^2 values for LDHs samples and the maximum capacities, the equilibrium data were better fit using the Langmuir isotherm (with a high correlation coefficient) rather than the Freundlich isotherm. The high coefficient values for the Langmuir isotherm indicate monolayer sorption of Cl^-, SO_4^{2-}, and CO_3^{2-} anions onto CaFe-LDHs.

3.6. Corrosion protection of steel rebars with and without CaFe-LDHs

To study the effect of CaFe-LDHs on the corrosion protection behavior of a steel rebar, potentiodynamic polarization (PDP) curves for samples with and without CaFe-LDHs formed by structural transformation in NaCl, Na_2SO_4, and Na_2CO_3 solution are shown in Fig. 8.

The values of electrochemical kinetic parameters such as corrosion potential (E_{corr}), corrosion current (I_{corr}), anodic and cathodic Tafel slopes (β_a and β_c), and corrosion rate (CR)

Table 3 Electrochemical polarization parameters and calculated corrosion rate (mm per year) without LDHs and with LDHs in NaCl, Na_2SO_4, and Na_2CO_3 (ionic species: 250 ppm)

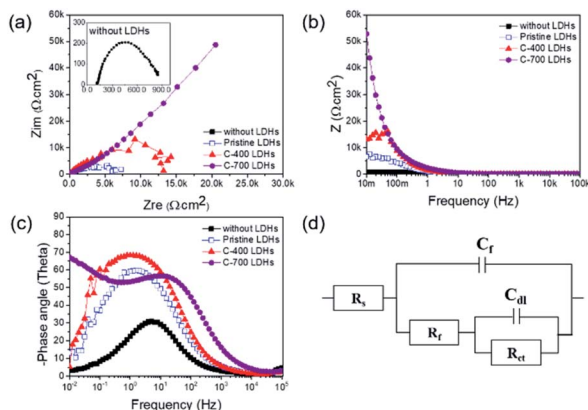| Sample	E_{corr} (mV)	I_{corr} (μA)	β_a (mV dec^{-1})	β_c (mV dec^{-1})	CR (mm per year)
Without LDHs	−298.57	161.73	1909.27	386.42	1876.56×10^{-3}
Pristine LDHs	−256.31	5.23	142.62	126.74	60.68×10^{-3}
C-400 LDHs	−220.31	0.38	81.53	55.61	4.41×10^{-3}
C-700 LDHs	−218.82	0.23	68.91	36.48	2.67×10^{-3}

Fig. 9 (a) Nyquist plots, (b) Bode plots, and (c) phase angle plots, performed at the corrosion potentials for NaCl, Na$_2$SO$_4$, and Na$_2$CO$_3$ (250 ppm solutions) without CaFe-LDHs and with CaFe-LDHs. (d) Equivalent electrical circuit (EEC) used to fit the electrochemical impedance data.

obtained from the curves by the extrapolation method are listed in Table 3.

The corrosion rates (mm per year) from polarization were calculated utilizing the equation below [eqn (16)]:

$$CR = \frac{I_{corr} \times K \times EW}{\rho \times A} \qquad (16)$$

Here, EW is the equivalent weight of Fe (27 g), K is the corrosion rate constant (3272 mm per year per A per cm), ρ is the density of Fe (g cm^{-3}), and A is the surface area of the electrode. The I_{corr} value of the case with CaFe-LDHs was noticeably lower that of the case without CaFe-LDHs. This means that the electrochemical reaction between the electrolyte and sample was reduced, decreasing the participation of electrons in the reaction. The CR value without CaFe-LDHs was 1876.56 × 10^{-3} mm per year for the steel rebar. This value remarkably decreased only because of the presence of CaFe-LDHs. Compared to the steel rebar without CaFe-LDHs, the CR values gradually decreased to 60.68 × 10^{-3} mm per year for pristine LDHs, and the structural modulations further enhanced the anti-corrosion effect to 2.67 × 10^{-3} mm per year for C-400 LDHs and to 2.67 × 10^{-3} mm per year for C-700 LDHs. In other words, the CR of C-700 LDHs (2.67 × 10^{-3} mm per year) implies that, when the steel rebar is exposed to a mixture of anionic species, the speed of steel corrosion is accelerated to 702.6 times faster than when it is protected by the C-700 LDHs (which present the best anion adsorption properties). As can be seen from the Nyquist plot of

rebar without and with CaFe-LDHs in Fig. 9(a). The diameter of the semicircle significantly increased for protective CaFe-LDHs. It is means that the resistance is increased and corrosion is reduced. The corrosion protection with CaFe-LDHs led to an obvious increase in the diameter of the capacitive loop,[53] as confirmed by Bode plots given in Fig. 9(c). The equivalent-circuit model constants in Fig. 9(d) were applied as these account for corrosion protection. In this equivalent circuit model, the steel rebar is considered to have a porous structure and to show capacitive behavior.[54–57] To compare the inhibition efficiencies (IE) with and without CaFe-LDHs, impedance parameters are shown in Table 4.

R_s refers to electrolyte resistance, R_f and C_f are electrolyte resistance inside pores and film capacitance, respectively. R_{ct} is the charge transfer resistance of electrochemical processes taking place inside the pores, and C_{dl} is the double-layer capacitance. Here, the C_{dl} value observed without LDHs was 524.80 (μF cm^{-2}), and this value generally decreased with use of CaFe-LDHs. Specifically, it decreased to 157.63 (μF cm^{-2}) for pristine LDHs, to 104.32 (μF cm^{-2}) for C-400 LDHs, and to 217.95 (μF cm^{-2}) for C-700 LDHs. This trend can be explained according to the Helmholtz model, where C_{dl} is expressed as [eqn (17)]:

$$C_{dl} = \frac{\varepsilon_r \varepsilon_0}{d} S \qquad (17)$$

Here, S is the exposed surface area of the steel specimen, d represents the thickness of the double layer, ε_r denotes the dielectric constant of the electrolyte inside the capacitor, and ε_0 is the vacuum dielectric constant. The steel rebar without CaFe-LDHs was expected to have a higher exposed surface area induced by destructive corrosion, leading to the increase in C_{dl} values compared to that with CaFe-LDHs. Because addition of CaFe-LDHs decreased the concentration of aggressive Cl$^-$, SO$_4^{2-}$, and CO$_3^{2-}$ anions, corrosion of the steel specimen was significantly reduced by decreasing the exposed surface area. In addition, it is well known that the IE of a steel rebar is inversely proportional to the R_{ct} value. In a solution without CaFe-LDHs, the R_{ct} value was 0.38 × 10^3 Ω cm^2. This value was increased to 5.41 × 10^3 Ω cm^2 by pristine LDHs, to 14.86 × 10^3 Ω cm^2 by C-400 LDHs, and to 218.97 × 10^3 Ω cm^2 by C-700 LDHs. To clearly illustrate the inhibition effect of CaFe-LDHs, the IE% of the CaFe-LDHs was calculated using the following equation [eqn (18)]:

$$IE\ (\%) = \frac{R_{ct,\ with\ LDH} - R_{ct,\ without\ LDH}}{R_{ct,\ with\ LDH}} \qquad (18)$$

Table 4 Impedance parameters and calculated inhibition efficiencies (IE%) without LDHs and with LDHs in NaCl, Na$_2$SO$_4$, and Na$_2$CO$_3$ solutions (ionic species: 250 ppm)

Sample	R_s (Ω cm^2)	C_f (μF cm^{-2})	R_f (Ω cm^2)	C_{dl} (μF cm^{-2})	R_{ct} (Ω cm^2)	IE (%)
Without LDHs	123.32	81.00	0.28 × 10^3	524.80	0.38 × 10^3	—
Pristine LDHs	71.02	73.70	0.67 × 10^3	157.63	5.41 × 10^3	93.03
C-400 LDHs	65.22	59.33	1.13 × 10^3	104.32	14.86 × 10^3	97.47
C-700 LDHs	57.20	58.51	217.97 × 10^3	217.95	218.97 × 10^3	99.83

Table 5 Comparison of LDHs removal capacity for anionic species obtained in previous reports by equilibrium sorption measurements

LDHs	Removal capacity of Cl^- (mg g^{-1})	Reference
C-700 LDHs	881.83	Our study
MgAl-LDHs	257.00	50
MgAl-LDHs	168.00	51
MgAl-LDHs	149.50	52
MgAl-LDHs	128.20	12

LDHs	Removal capacity of SO_4^{2-} (mg g^{-1})	Reference
C-700 LDHs	706.21	Our study
MgAl-LDHs	144.09	17
Zn–Al LDHs	98.13	53
Mg–Fe LDHs	68.73	54

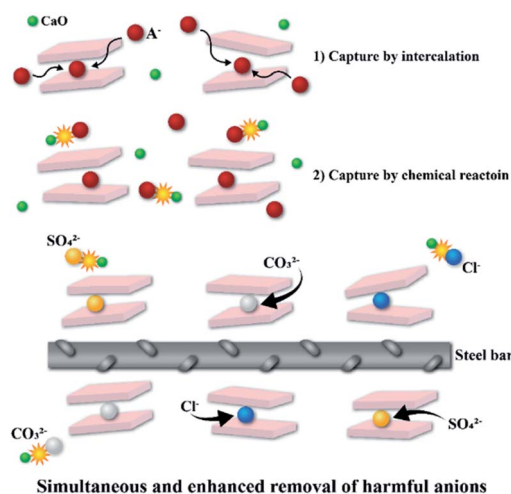| LDHs	Removal capacity of CO_3^{2-} (mg g^{-1})	Reference
C-700 LDHs	879.73	Our study

Here, $R_{ct, \text{ with CaFe-LDHs}}$ and $R_{ct, \text{ without CaFe-LDHs}}$ are the charge transfer resistances for the steel specimens in the presence and absence of the CaFe-LDHs, respectively. According to Table 4, the solution containing the steel specimen and CaFe-LDHs showed inhibition effects. Specifically, the highest IE% (99.83%) was obtained when C-700 LDHs was applied.

3.7. Synergy of simultaneous adsorption of anions and corrosion prevention in steel rebar by CaFe-LDHs with structural modulation

Rapid removal of harmful anions not long after their introduction into the aqueous solution or into the matrix of steel-reinforced concrete is crucial for coating materials or anti-corrosion additives. This property can be related to (1) adsorption rate of anions (i.e., removal percentage of anions (%) per given reaction time [see Section 4.2]) and (2) removal capacity (i.e., maximum amount of ionic species removed (mg) per unit mass of LDHs (g) [see Section 4.5]). The anion removal performance is more distinct when we compare the removal capacity of C-700 LDHs with previously released reports (Table 5).

The Q_{max} for Cl^- was 881.83 mg g^{-1}, which is over 3.4 times that of previous studies. Furthermore, the value for SO_4^{2-} (706.21 mg g^{-1}) was over 5.69 times higher than previous reports.[11,16,58–62] The value for CO_3^{2-} was 879.73 mg g^{-1}, which was not previously reported. In addition, no comparable result has been observed in terms of removal capacity of CO_3^2.

This synergy was induced by (1) anion capture by reconstruction (2) capture by chemical reaction with metal oxide (see Fig. 10). 1 mole of pristine LDHs with crystallinity of Ca$_2$Fe(OH)$_6$(NO$_3$)·2H$_2$O can exchange 1 mole of monovalent anion including Cl^- with NO_3^-, while C-700 LDHs can capture 4 moles of Cl^-, 1.5 moles of SO_4^{2-}, and 1.5 moles of CO_3^{2-} [also see eqn (6)–(11)]. Here, 1 mole of Cl^- ions was captured by intercalation

Fig. 10 Adsorption and corrosion protection mechanism of C-700 LDHs with different anions; Cl^-, SO_4^{2-} and CO_3^{2-}.

between cationic layers during the refolding process, and another 3 moles of Cl^- ions were captured by chemical reaction with CaO, which was generated during thermal treatment at 700 °C. This metal oxide moiety, initiated by pristine-LDHs, also captures Cl^-, SO_4^{2-} or CO_3^{2-} ions by chemical reaction other than capturing by the refolding process, which cannot be realized even after calcination of typical Mg–Al-LDHs or Ca–Al-LDHs.[63] This enhanced adsorption of ionic species in aqueous solution reduced corrosion in the steel specimen in water because of prompt removal of corrosion sources Cl^- and SO_4^{2-}, as well as another deleterious anion, CO_3^{2-}, upon introduction to reaction media or building matrix.

Hence, the enhanced removal performance of Cl^-, SO_4^{2-}, and CO_3^{2-} and anti-corrosion effects by CaFe-LDH-induced crystalline structures utilized in this work suggest that CaFe-LDHs are promising materials for superior corrosion protection in concrete structures.

4. Conclusions

In this study, we fabricated CaFe-LDHs by structural transformation, demonstrated their simultaneous removal of destructive anions (Cl^-, SO_4^{2-}, and CO_3^{2-}) in aqueous solutions and superior anti-corrosion efficiency. In the investigation of adsorption kinetics, pseudo-second-order kinetics and Langmuir isotherm models well fit the data, which confirms that the target anions were effectively removed with the CaFe-LDHs predominantly by chemisorption through monolayer sorption. Compared with previous reports, the removal capacity (Q_{max}) of C-700 LDHs was remarkably enhanced. The Q_{max} of Cl^- (881.83 mg g^{-1}) was over 3.4 times that of previous work, while that of SO_4^{2-} (706.21 mg g^{-1}) was over 5.69 times that of previous literature. This corrosion inhibition efficiency by C-700 LDHs reached 98.83% compared to that of bare rebar without LDHs. This synergy was induced by (1) anion capture by reconstruction (2) capture by chemical reaction with metal oxide of C-700 LDHs.

Our data show that the durability and sustainability of buildings can be enhanced by employing the CaFe-LDHs as a coating material, filler in concrete, or additive in the construction industry.

Conflicts of interest

There are no conflicts to declare.

Acknowledgements

Notes and references

1 H. Shirkhani, J. Y. Zhang and Z. Lounis, *Nat. Hazards Rev.*, 2020, **21**, 1–14.

2 M. R. Geiker, A. Michel, H. Stang and M. D. Lepech, *Cem. Concr. Res.*, 2019, **122**, 189–195.

3 R. E. Melchers, *J. Mar. Sci. Eng.*, 2020, **8**, 1–12.

4 F. Winnefeld, M. Ben Haha, G. Le Saout, M. Costoya, S.-C. Ko and B. Lothenbach, *J. Sustainable Cem.-Based Mater.*, 2014, **4**, 85–100.

5 S. D. Wang, K. L. Scrivener and P. L. Pratt, *Cem. Concr. Res.*, 1994, 1033–1043.

6 S. Song, D. Sohn, H. Jennings and T. Mason, *J. Mater. Sci.*, 2000, **35**, 249–257.

7 M. Moreno, W. Morris, M. G. Alvarez and G. S. Duffó, *Corros. Sci.*, 2004, **46**, 2681–2699.

8 Z. Dong and A. Poursaee, *Constr. Build. Mater.*, 2020, **240**, 117955.

9 H. S. Wang, X. Cao, H. K. Gu, Y. Y. Liu, Y. B. Li, Z. W. Zhang, W. Huang, H. X. Wang, J. Y. Wang, W. Xu, J. G. Zhang and Y. Cui, *ACS Nano*, 2020, **14**, 4601–4608.

10 K. Wang, H. X. Chen, X. F. Zhang, Y. X. Tong, S. Q. Song, P. Tsiakaras and Y. Wang, *Appl. Catal., B*, 2020, **264**, 118468.

11 J. Zuo, B. Wu, C. Luo, B. Dong and F. Xing, *Corros. Sci.*, 2019, **152**, 120–129.

12 A. M. Neville, *Properties of concrete*, Pearson, Edinburgh, England, 5th edn, 2011.

13 Z. Yang, H. Fischer and R. Polder, *Mater. Corros.*, 2013, **64**, 1066–1074.

14 B.-G. Paik, G.-D. Kim, K.-Y. Kim, H.-S. Seol, B.-S. Hyun, S.-G. Lee and Y.-R. Jung, *Ocean Eng.*, 2013, **73**, 139–148.

15 Y. Ben Amor, L. Bousselmi, H. Takenouti and E. Triki, *Corros. Eng., Sci. Technol.*, 2005, **40**, 129–135.

16 J. Xu, Q. Tan and Y. Mei, *Corros. Sci.*, 2020, **163**, 108223.

17 Y.-z. Zhang, Y.-f. Fan and H.-n. Li, *Int. J. Corros.*, 2012, **2012**, 1–7.

18 N. Kabashi, C. Krasniqi, A. Sadikaj, S. Bublaku, M. Ali and H. Morina, *Corrosion In Concrete Under Sulphate And Chloride Attacks*, 2017.

19 C. Qian, R. Li, M. Luo and H. Chen, *J. Wuhan Univ. Technol., Mater. Sci. Ed.*, 2016, **31**, 557–562.

20 A. Królikowski and J. Kuziak, *Electrochim. Acta*, 2011, **56**, 7845–7853.

21 T. T. X. Hang, T. A. Truc, N. T. Duong, N. Pébère and M.-G. Olivier, *Prog. Org. Coat.*, 2012, **74**, 343–348.

22 M. Xu and M. Wei, *Adv. Funct. Mater.*, 2018, **28**, 1802943.

23 X. Mei, R. Liang, L. Peng, T. Hu and M. Wei, *J. Mater. Chem. B*, 2017, **5**, 3212–3216.

24 L. P. Cardoso, R. Celis, J. Cornejo and J. B. Valim, *J. Agric. Food Chem.*, 2006, **54**, 5968–5975.

25 Z. M. Mir, A. Bastos, D. Hoche and M. L. Zheludkevich, *Adv. Eng. Mater.*, 2020, 2000398.

26 G. Mishra, B. Dash and S. Pandey, *Appl. Clay Sci.*, 2018, **153**, 172–186.

27 K. L. Erickson, T. E. Bostrom and R. L. Frost, *Mater. Lett.*, 2005, **59**, 226–229.

28 Z. Gao, K. Sasaki and X. Qiu, *Langmuir*, 2018, **34**, 5386–5395.

29 S. Mondal, S. Dasgupta and K. Maji, *Mater. Sci. Eng.*, 2016, **68**, 557–564.

30 Q. Wang, Y. Gao, J. Luo, Z. Zhong, A. Borgna, Z. Guo and D. O'Hare, *RSC Adv.*, 2013, **3**, 3414–3420.

31 J. L. Chen, L. Fang, F. Wu, X. G. Zeng, J. Hu, S. F. Zhang, B. Jiang and H. J. Luo, *Trans. Nonferrous Met. Soc. China*, 2020, **30**, 2424–2434.

32 F. Zhang, C. L. Zhang, L. Song, R. C. Zeng, Z. G. Liu and H. Z. Cui, *Trans. Nonferrous Met. Soc. China*, 2015, **25**, 3498–3504.

33 J. L. Chen, L. Fang, F. Wu, J. Xie, J. Hu, B. Jiang and H. J. Luo, *Prog. Org. Coat.*, 2019, **136**, 105234.

34 M. A. Iqbal and M. Fedel, *Surf. Coat. Technol.*, 2018, **352**, 166–174.

35 S. K. Poznyak, J. Tedim, L. M. Rodrigues, A. N. Salak, M. L. Zheludkevich, L. F. Dick and M. G. Ferreira, *ACS Appl. Mater. Interfaces*, 2009, **1**, 2353–2362.

36 L. Yang, M. Chen, Z. Lu, Y. Huang, J. Wang, L. Lu and X. Cheng, *Cem. Concr. Compos.*, 2020, **114**, 103817.

37 N. Jahanzeb, J.-H. Shin, J. Singh, Y.-U. Heo and S.-H. Choi, *Mater. Sci. Eng. A*, 2017, **700**, 338–350.

38 M. Al-Jaberi, S. Naille, M. Dossot and C. Ruby, *J. Mol. Struct.*, 2015, **1102**, 253–260.

39 G. Varga, V. Kozma, V. J. Kolcsár, Á. Kukovecz, Z. Kónya, P. Sipos, I. Pálinkó and G. Szőllősi, *Mol. Catal.*, 2020, **482**, 110675.

40 M. Szabados, Z. Kónya, Á. Kukovecz, P. Sipos and I. Pálinkó, *Appl. Clay Sci.*, 2019, **174**, 138–145.

41 M. Taei, E. Havakeshian, H. Salavati and F. Abedi, *RSC Adv.*, 2016, **6**, 27293–27300.

42 Y. Xu, H. Hou, Q. Liu, J. Liu, L. Dou and G. Qian, *Desalin. Water Treat.*, 2015, **57**, 7918–7925.

43 Y. Wu, Y. Yu, J. Z. Zhou, J. Liu, Y. Chi, Z. P. Xu and G. Qian, *Chem. Eng. J.*, 2012, **179**, 72–79.

44 F. Z. Mahjoubi, A. Khalidi, M. Abdennouri and N. Barka, *Journal of Taibah University for Science*, 2017, **11**, 90–100.

45 N. Butto, G. Cabrera-Barjas and A. Neira-Carrillo, *Crystals*, 2018, **8**, 82.

46 C. Gomes, Z. Mir, A. C. Bastos, F. Maia, C. Rocha, J. Tedim, M. L. Zheludkevich and M. Ferreira, *Effect of Layered Double Hydroxides on the Performance and Service Life of Reinforced Concrete*, 2019.

47 H.-m. Zhang, S.-h. Zhang, P. Stewart, C.-h. Zhu, W.-j. Liu, A. Hexemer, E. Schaible and C. Wang, *Chin. J. Polym. Sci.*, 2016, **34**, 542–551.

48 T. Ishizaki, S. Chiba, K. Watanabe and H. Suzuki, *J. Mater. Chem. A*, 2013, **1**, 8968–8977.

49 G. Mishra, B. Dash and S. Pandey, *Appl. Clay Sci.*, 2018, **153**, 172–186.

50 L. Moyo, N. Nhlapo and W. W. Focke, *J. Mater. Sci.*, 2008, **43**, 6144–6158.

51 S. Marappa, R. Shivaramaiah and P. Vishnu, *Eur. J. Inorg. Chem.*, 2013, **2013**, 2122–2128.

52 T. A. Saleh, A. M. Muhammad and S. A. Ali, *J. Colloid Interface Sci.*, 2016, **468**, 324–333.

53 W. Lee, R. Ji, U. Gösele and K. Nielsch, *Nat. Mater.*, 2006, **5**, 741–747.

54 J. Xu, Q. Tan and Y. Mei, *Corros. Sci.*, 2020, **163**, 108223.

55 I. Imanieh and A. Afshar, *J. Mater. Res. Technol.*, 2019, **8**, 3004–3023.

56 L. F. Hou, Y. L. Li, J. L. Sun, S. H. Zhang, H. Wei and Y. H. Wei, *Appl. Surf. Sci.*, 2019, **487**, 101–108.

57 A. Liu, X. Ju, H. Tian, H. Yang and W. Li, *Appl. Surf. Sci.*, 2019, **493**, 239–249.

58 S. Yoon, J. Moon, S. Bae, X. Duan, E. P. Giannelis and P. M. Monteiro, *Mater. Chem. Phys.*, 2014, **145**, 376–386.

59 L. Lv, J. He, M. Wei, D. G. Evans and X. Duan, *Water Res.*, 2006, **40**, 735–743.

60 Y. Zhao, W. Hu, J. Chen and L. Lv, *Desalin. Water Treat.*, 2012, **36**, 50–56.

61 S. Iftekhar, M. E. Kucuk, V. Srivastava, E. Repo and M. Sillanpaa, *Chemosphere*, 2018, **209**, 470–479.

62 J. Liu, X. Yue, Y. Yu and Y. Guo, *Desalin. Water Treat.*, 2014, **56**, 274–283.

63 X. Ke, S. A. Bernal and J. L. Provis, *Cem. Concr. Res.*, 2017, **100**, 1–13.